Antibody-guided photoablation of voltage-gated potassium currents

Jon T. Sack,[1,2,3] Nicholas Stephanopoulos,[4] Daniel C. Austin,[1] Matthew B. Francis,[4] and James S. Trimmer[1,2]

[1]Department of Physiology and Membrane Biology and [2]Department of Neurobiology, Physiology, and Behavior, University of California, Davis, Davis, CA 95616
[3]Protean Research, Institute for Design of Intelligent Drugs, Palo Alto, CA 94306
[4]Department of Chemistry, University of California, Berkeley, Berkeley, CA 94704

A family of 40 mammalian voltage-gated potassium (Kv) channels control membrane excitability in electrically excitable cells. The contribution of individual Kv channel types to electrophysiological signaling has been difficult to assign, as few selective inhibitors exist for individual Kv subunits. Guided by the exquisite selectivity of immune system interactions, we find potential for antibody conjugates as selective Kv inhibitors. Here, functionally benign anti-Kv channel monoclonal antibodies (mAbs) were chemically modified to facilitate photoablation of K currents. Antibodies were conjugated to porphyrin compounds that upon photostimulation inflict localized oxidative damage. Anti-Kv4.2 mAb–porphyrin conjugates facilitated photoablation of Kv4.2 currents. The degree of K current ablation was dependent on photon dose and conjugate concentration. Kv channel photoablation was selective for Kv4.2 over Kv4.3 or Kv2.1, yielding specificity not present in existing neurotoxins or other Kv channel inhibitors. We conclude that antibody–porphyrin conjugates are capable of selective photoablation of Kv currents. These findings demonstrate that subtype-specific mAbs that in themselves do not modulate ion channel function are capable of delivering functional payloads to specific ion channel targets.

The Journal of General Physiology

INTRODUCTION

Voltage-gated potassium (Kv) channels play diverse roles including controlling the repolarization phase of action potentials in electrically excitable cells throughout the brain and body. In mammals, Kv channels arise from a family of 40 genes encoding pore-forming subunits (Gutman et al., 2005). This genetic diversity is greater than any other family of ion channels, and individual cells express an array of different Kv types. Each channel type has a distinct subcellular distribution and functional properties to make a unique contribution to electrical signaling (Vacher et al., 2008). Selectively inhibiting Kv subtypes is a promising method of tuning electrical excitability for research and clinical purposes, yet has been difficult in practice.

The diversity of Kv channels poses a challenge to biomedical science. The contribution to electrical signaling of any individual channel type is difficult to conclusively demonstrate. Hence, the precise physiological function of most Kv subunits remains unknown. For most Kv subunits, drugs of great selectivity have not yet been discovered. In the rare cases where selective Kv inhibitors have been found, they have proven indispensable in identifying channel functions. For example, extensive efforts to develop pharmacology selective for Kv channels in human T lymphocytes (DeCoursey et al., 1984; Grissmer et al., 1990; Lin et al., 1993) led to the identification of the pivotal role of Kv1.3 in immune activation, and the channel is now the target of several drugs in clinical trials (Beeton et al., 2006; Tarcha et al., 2012). For most Kv channels, researchers rely on a patchwork pharmacology insufficient to conclusively identify the function of specific channel types. Because of the inadequacy of subtype-selective Kv drugs, the limiting step in developing Kv therapies remains the process of identifying a specific channel type as a target for drug development, or "target validation" (Kaczorowski et al., 2008; Rhodes and Trimmer, 2008). Ideally, to identify the physiological roles of Kv channels, a selective drug would be available for every Kv type.

Selective antibodies have been developed against most Kv subunits (Vacher et al., 2008). However, generation of antibodies that inhibit ionic current has proven difficult. There are several publications describing inhibitory antibodies that target Kv subunits (Zhou et al., 1998; Murakoshi and Trimmer, 1999; Jiang et al., 2003; Xu et al., 2006; Gómez-Varela et al., 2007; Yang et al., 2012), but none of these antibodies has yet emerged with the qualities required for widespread use (Dallas et al., 2010). What would be most useful to researchers are mAbs against extracellular epitopes that robustly modulate function of mammalian Kv channels.

Correspondence to Jon T. Sack: jsack@ucdavis.edu

Abbreviations used in this paper: Kv, voltage-gated potassium; PB, sodium phosphate buffer.

The Rockefeller University Press $30.00
J. Gen. Physiol. Vol. 142 No. 3 315–324
www.jgp.org/cgi/doi/10.1085/jgp.201311023

We have generated several mAbs that bind epitopes on the external face of Kv channels. These exhibit clear specificity for Kv subtypes, including Kv1.1 (Tiffany et al., 2000), Kv2.1 (Lim et al., 2000), and Kv4.2 (Shibata et al., 2003). None of these mAbs has been found to inhibit currents. Our objective is to harness the exquisite selectivity of these mAbs to selectively modulate Kv function. By attaching inhibitory moieties to subtype-selective mAbs, we aim to find a solution to the problematic scarcity of selective Kv inhibitors that can be applied to all subtypes.

In this communication, we report a means of imbuing benign anti-Kv mAbs with inhibitory potency. Our strategy for targeted inhibition of Kv channels was to label antibodies with chromophores that induce oxidative damage to the target protein upon photostimulation. Such strategies have proven useful to permanently inhibit proteins (Beck et al., 2002; Lee et al., 2008). Related strategies involving genetically targeted photosensitizers have also proven to be a viable means of inhibiting membrane proteins including ion channels and aquaporins (Tour et al., 2003; Baumgart et al., 2012). In all of these strategies, photostimulation of certain chromophores leads to the local generation of reactive oxygen species. The lifetime of the reactive species determines its diffusional distance and hence a radius of localized oxidative damage. One extensively used species is singlet oxygen, which has an ~40-Å half-maximal radius of oxidative damage (Beck et al., 2002; Vegh et al., 2011). Oxidative damage mediated by singlet oxygen has proven capable of ablating the function of a wide range of protein targets but also results in varying degrees of collateral damage to other cell components (Guo et al., 2006). As the use of efficient reactive oxygen–generating species may help minimize unintended damage, we sought to find chromophores with optimal properties. In this work, we test the capacity of porphyrin conjugates to mediate photoablation of ionic currents. Porphyrins are among the most efficient photo-induced generators of singlet oxygen known. For example, 5,10,15,20-tetrakis (1-methylpyridinium-4-yl)porphine, which is closely related to the photosensitizer, 1, used here (Fig. 2 A), has a singlet oxygen quantum yield in water of 0.74 (Verlhac et al., 1984). This is far higher than the quantum yield of 0.03–0.06 reported for fluorescein (Wilkinson et al., 1993), which is classically used for targeted photoablation of protein function (Redmond and Gamlin, 1999; Smith et al., 2011). Additionally, as with most porphyrins, our photosensitizer, 1, has a greater maximal extinction coefficient, $\varepsilon_{425\ nm} = 220{,}000\ M^{-1}\ cm^{-1}$ (Tomé et al., 2004), than fluorescein, $\varepsilon_{490\ nm} = 76{,}900\ M^{-1}\ cm^{-1}$ (Sjoback et al., 1998). Because of their efficient photostimulated generation of reactive oxygen, porphyrins are used clinically in photodynamic therapy for cancer treatment (Bonnett, 1995; Agostinis et al., 2011). We have previously used virus capsids loaded with porphyrins to target cancer cells (Stephanopoulos et al., 2010), and there are reports of mAbs targeting porphyrins to cancer cells (Alonso et al., 2010; Palumbo et al., 2011). Here, we target porphyrin photosensitizers with subtype-specific mAbs. We find that currents from Kv channels can be selectively ablated by photostimulation of antibody-conjugated porphyrins.

MATERIALS AND METHODS

Antibody validation

To target photoinhibitors to Kv channels, an extensively validated, subtype-selective anti-Kv mAb was chosen. The IgG1 clone K57/1 (Shibata et al., 2003) was found to be selective for mammalian Kv4.2 channels (Rhodes et al., 2004; Menegola and Trimmer, 2006), has been used for studies by multiple research groups (Burkhalter et al., 2006; Gardoni et al., 2007; Kim et al., 2007; Amarillo et al., 2008; Hammond et al., 2008), and is publicly available from the UC Davis/National Institutes of Health NeuroMab facility. The K57/1 mAb was generated against a synthetic peptide, "Kv4.2e," that mimicked amino acids of the external loop between the S1 and S2 segment of the human Kv4.2 subunit (Fig. 1 A). The S1–S2 linker is the longest and most variable external region of Kv proteins and, as such, is an attractive target for generating subtype-specific externally acting antibodies. The Kv4.2e sequence is identical in human, rat, mouse, and other mammalian Kv4.2 orthologues. The K57/1 antibody is highly specific for Kv4.2 over its closely related family members Kv4.1 and Kv4.3 (Rhodes et al., 2004). K57/1 exhibits robust binding in immunohistochemical staining of the intact brains and in immunoblot analyses of denatured protein samples prepared from wild-type mice did not exhibit detectable signals in Kv4.2 knockout mice (Fig. 2, B and C) (Menegola and Trimmer, 2006). To date, all anti-Kv channel S1–S2 linker antibodies we have tested, including the K57/1 mAb, have proven ineffectual as inhibitors of their targeted Kv channels (Fig. 1 D).

Immunoblots

All animals were cared for and euthanized in accordance with institutional animal use protocols. Rat and mouse brain membranes were prepared as described previously (Shi et al., 1994). Mouse brain membranes were prepared from brains of Kv4.2 knockout mice (Guo et al., 2005) and wild-type littermates. In brief, brains from adult rats and mice were homogenized in 5 mM sodium phosphate buffer (PB), pH 7.4, containing 320 mM sucrose and 100 mM NaF. The homogenate was centrifuged at 800 *g* for 10 min to remove nuclei and unbroken tissues, and then centrifuged at 100,000 *g* to prepare a membrane fraction. Membranes were diluted with the sample buffer for SDS-PAGE. Molecular weight standards were Amersham Rainbow Markers (RPN800). Proteins were separated by SDS-PAGE on 7.5% gels, transferred to nitrocellulose membranes, and immunoblotted with anti-Kv4.2 K57/1 or anti-Kv2.1 K89/41 (Antonucci et al., 2001) mouse mAb tissue culture supernatants at 1:2. The blots were incubated with horseradish peroxidase–conjugated secondary antibodies (MP Biomedicals), followed by enhanced chemiluminescence reagent (PerkinElmer). Immunoreactive bands were visualized by exposing the blot to x-ray film.

Immunofluorescence staining of brain sections

Mice were deeply anesthetized with sodium pentobarbital (60 mg/kg, intraperitoneally) and perfused through the ascending aorta with 20 ml of 0.9% saline, followed by 80 ml of fixative containing 4% formaldehyde, prepared from freshly depolymerized paraformaldehyde, in 0.1 M PB. The brains were removed, cryoprotected

for 18–48 h in 20% sucrose, frozen in a bed of pulverized dry ice, and then cut into 40-µm sagittal sections on a sliding microtome (Michrom HM 450; Richard-Allan Scientific) equipped with a freezing stage (BFS-30TC and PTU-3; Physitemp). Sections were collected in 0.1 M PB and processed immediately for immunohistochemistry as described below.

For immunohistochemistry, sections were washed four times for 5 min each in ice cold 0.1 M PB and blocked for 1 h at 4°C in vehicle (10% goat serum, 0.1 M PB, and 0.3% Triton X-100). Sections were incubated overnight at 4°C in vehicle containing anti-Kv4.2 mouse mAb K57/1 and anti-Kv2.1 affinity-purified rabbit polyclonal antibody KC (Trimmer, 1991). Sections were washed four times for 5 min each in vehicle and incubated for 1 h in vehicle containing affinity-purified, species-specific goat secondary antibodies conjugated to Alexa Fluors (Life Technologies). Sections were then washed again for 5 min each in vehicle, 0.1 M PB, and 0.05 M PB, and mounted on gelatin-coated slides, dried, and coverslipped using mounting medium (ProLong Gold; Life Technologies).

Fluorescence images were taken using the same exposure time for each set of samples to directly compare the signal intensity. Images were acquired with a charge-coupled device camera installed on an Axiovert 200-M microscope with a 20×, 0.8 numerical aperture lens, and an ApoTome coupled to Axiovision software (Carl Zeiss). Images were exported from Axiovision as TIFF or JPEG files and imported into Photoshop (Adobe).

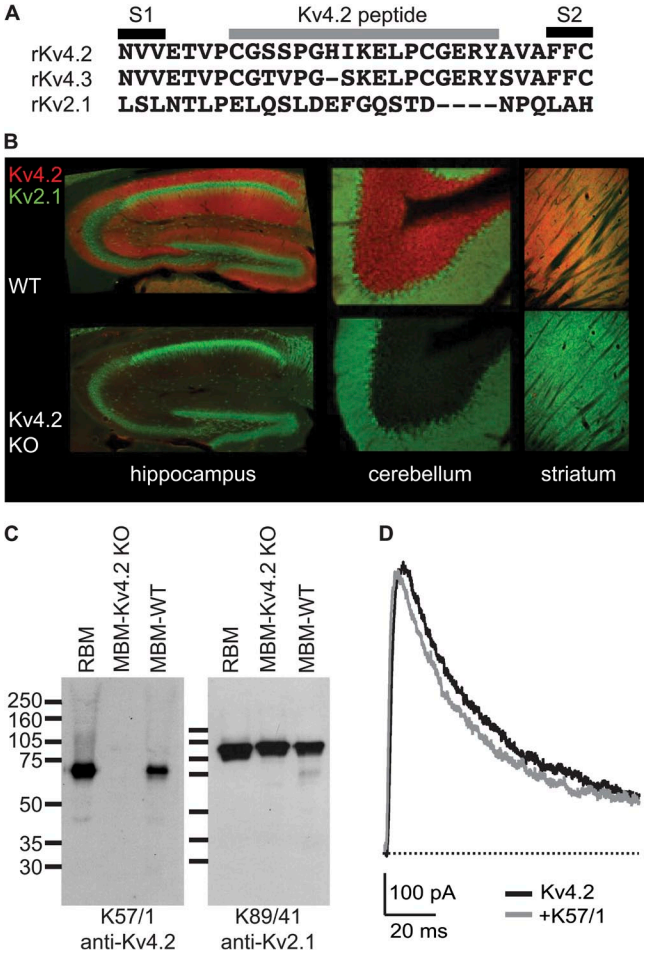

Figure 1. Validation of anti-Kv4.2 mAb. (A) Sequence alignment of relevant K channels indicating residues included in Kv4.2 immunogenic peptide. (B) Immunohistochemical analysis of antibody specificity in brain. Double-label immunofluorescence staining for anti-Kv4.2 mAb (red) and anti-Kv2.1 polyclonal antibody (green) in sections prepared from the brains of wild-type (top row) and Kv4.2 knockout (bottom row) mice. (C) Immunoblot analysis of antibody specificity in brain. Immunoblot of adult rat brain membranes (RBM), adult mouse brain membranes from Kv4.2 knockout (MBM-Kv4.2-KO), and wild-type (MBM-WT) mice probed with anti-Kv4.2 or anti-Kv2.1 mAbs as noted. Numbers to the left denote mobility of prestained molecular weight standards in kilodaltons. (D) Whole cell Kv4.2 current from a 0-mV pulse before and 8 min after the application of 1 µM anti-Kv4.2 mAb K57/1 to a HEK cell. P/5 subtraction was used to isolate K currents.

Porphyrin synthesis and antibody conjugation

To imbue antibodies with photoinhibitory functionality, water-soluble porphyrin compounds were synthesized and functionalized for conjugation to proteins. The porphyrin ring is aromatic and hydrophobic, with sparing water solubility. The porphyrins used in this work were chemically altered to increase their hydrophilicity by appending charged moieties to three of the four aryl groups projecting from the porphyrin ring. Positive charges were introduced by using methylated pyridine derivatives, and negative charges were introduced by attaching sulfonate groups to the aryl rings (Fig. 2 A). The fourth aryl group projecting from the porphyrin core was engineered for linkage to antibodies. Porphyrins were synthesized for three conjugation strategies: porphyrin 1 for *N*-hydroxysuccinimide–mediated addition to mAb primary amine groups (e.g., lysines); porphyrin 2 for isothiocyanate-mediated addition to primary amine groups; and porphyrin 3 for the conjugation of aminooxy groups to aldehydes/ketones introduced into the antibody amino termini using a pyridoxal-6-phosphate–mediated transamination reaction (Gilmore et al., 2006; Scheck and Francis, 2007). Water-soluble porphyrins were reacted with K57/1 antibody (Fig. 2 B), and these antibody–porphyrin conjugates tested for photoinhibitory activity against Kv channels.

Cationic porphyrin-NHS ester 1 (Fig. 2 A) was prepared according to a published procedure (Tomé et al., 2004). The final product was stored at −20°C as a 10-mM solution in DMSO. Anti-Kv4.2 antibody porphyrin 1 conjugate (αKv4.2•1) was prepared as follows: anti-Kv4.2 mAb K57/1 (Shibata et al., 2003) was initially purified from ascites fluid, as described previously (Trimmer et al., 1985). The antibody was further purified by elution from protein G sepharose (GE Healthcare), with 0.5 M acetic acid, neutralization with 0.6 volumes of 1 M sodium phosphate, pH 8.0, concentration in a centrifugal filter unit (30 K Amicon-4; EMD Millipore), and dialysis against 100 mM sodium phosphate, pH 8. In an opaque black polypropylene tube, with precautions taken to minimize light exposure, purified mAb (7 µM) was mixed with 16 equivalents of cationic porphyrin-NHS in DMSO, for 10% final DMSO concentration. The reaction vessel was purged with argon, and the reaction allowed to proceed for 3 h at 4°C, before termination by application to a desalting resin (Zeba; Thermo Fisher Scientific) preequilibrated with 150 mM NaCl and 10 mM PB, pH 7.3. The degree of antibody modification was approximately two porphyrins per antibody molecule, as determined from absorbance readings (Fig. 2 C) on wavelength-scanning spectrophotometer (Cary 50 Scan; Varian) using extinction coefficients (M^{-1} cm^{-1}) porphyrin 1, $\varepsilon_{280\ nm}$ = 10,000 and $\varepsilon_{425\ nm}$ = 220,000, and IgG, $\varepsilon_{280\ nm}$ = 210,000. This mAb–porphyrin conjugate, αKv4.2•1, was protected from light and stored with 1% BSA (03117332001; Roche) and 10 mM sodium azide at 4°C until use.

Anionic porphyrin isothiocyanate 2 (Fig. 2 A) was synthesized from 5-(4-aminophenyl)-10,15,20-tris(4-sulfonatophenyl)porphyrin, tris(*n*-tetrabutylamminonium) salt, according to published procedures (Endo et al., 2007; Stephanopoulos et al., 2009) as follows: the starting porphyrin (16 mg, 0.01 mmol) was dissolved in 4 ml anhydrous dichloromethane (DCM). To this solution was

added 1,1′-thiocarbonyldi-2(1*H*)-pyridone (5 mg, 0.02 mmol) in 1 ml DCM. The reaction was stirred at room temperature and reacted to completion in 2 h, as monitored by matrix-assisted laser desorption/ionization–time of flight (MALDI-TOF) mass spectroscopy. The solvent was removed under reduced pressure. The crude mixture was dissolved in DCM and product purified by silica gel chromatography, first using 10% methanol in DCM to elute unreacted pyridone, and then 50% methanol in DCM to elute the porphyrin. Product purity was verified by MALDI-TOF mass spectrometry. Solvent was removed under reduced pressure, and the porphyrin was stored at −20°C as a 20-mM solution in DMSO. To the purified K57/1 antibody (7 µM) in 0.5 M sodium bicarbonate, pH 9.2, 16 equivalents of anionic porphyrin 2 in DMSO were added, for a 10% final concentration of DMSO. The reaction vessel was purged with argon, and reaction was allowed to proceed for 1 h on ice. This conjugate, αKv4.2•2, was prepared as described above for αKv4.2•1.

Anionic porphyrin alkoxyamine 3 (Fig. 2 A) was prepared as described previously (Stephanopoulos et al., 2009) and was stored in DMSO until use. For conjugation to the antibody, it was first necessary to generate a ketone at the amino terminus of the antibody using a pyridoxal 5′-phosphate–based transamination reaction, as described previously (Gilmore et al., 2006). In brief, the K57/1 antibody (7 µM) in 50 mM phosphate buffer, pH 6.5, was exposed to 10 mM pyridoxal 5′-phosphate and allowed to react overnight at room temperature. The reaction was terminated by application to a desalting resin (Zeba; Thermo Fisher Scientific) prequilibrated with 150 mM NaCl and 10 mM PB, pH 7.3. To this transaminated antibody, 10 equivalents of anionic porphyrin 3 in DMSO were added, for a 10% final concentration of DMSO. The reaction vessel was purged with argon, and reaction was allowed to proceed overnight at room temperature. This conjugate, αKv4.2•3, was prepared as described above for αKv4.2•1.

ELISAs

The anti-Kv4.2 mAb K57/1 was generated against a synthetic peptide, Kv4.2e, CGSSPGHIKELPSGERY, in which the second cysteine from the corresponding Kv4.2 sequence (Fig. 1 A) was changed to serine for chemistry considerations (Shibata et al., 2003). The Kv4.2e peptide was conjugated to BSA by its amino-terminal cysteine and prepared as follows: a 0.5-ml aliquot of 10 mg/ml BSA dialyzed against 50 mM sodium phosphate, pH 6.0, was incubated with 800 µg sulfo-MBS (Thermo Fisher Scientific) on a tube rotator at room temp for 30 min. The product was passed through a G-50 column (Sephadex) equilibrated in 50 mM sodium phosphate, pH 6.0, to remove unconjugated sulfo-MBS. The peak 1-ml BSA fraction was added to 5 mg synthetic peptide dissolved in 0.5 ml of 1 mM EDTA and 20 mM sodium phosphate, pH 7.2, and rotated overnight at room temperature; aliquots were stored at −20°C until use.

96-well microtiter plates (655081; Greiner) were coated with 50 µl of 50 µg/ml Kv4.2e-BSA conjugate or a BSA control in 10 mM sodium azide overnight at 4°C. After a 45-min block with blotto (20 mM Tris HCl, pH 8, 150 mM NaCl, 4% nonfat dry milk, and 0.1% Tween 20) at room temperature, 50-µl primary antibody dilutions in blotto ± blocking peptide were added to wells and rocked gently for 45 min at room temperature. The 1° antibody solution was removed, and wells were washed with blotto three times at 5-min intervals, followed by a 45-min incubation with goat anti–mouse heavy and light chain–specific 2° antibody–horseradish peroxidase conjugate (KPL 474–1806) diluted at 1:5,000 in blotto. Wells were then washed three times at 5-min intervals with PBS (150 mM NaCl and 10 mM sodium phosphate, pH 7) and developed in 50 µl 3,3′,5,5′-tetramethylbenzidine solution (34028; Thermo Fisher Scientific) for 5 min before stop with 50 µl of 2 M sulfuric acid. Absorbance at 450 nm was quantified.

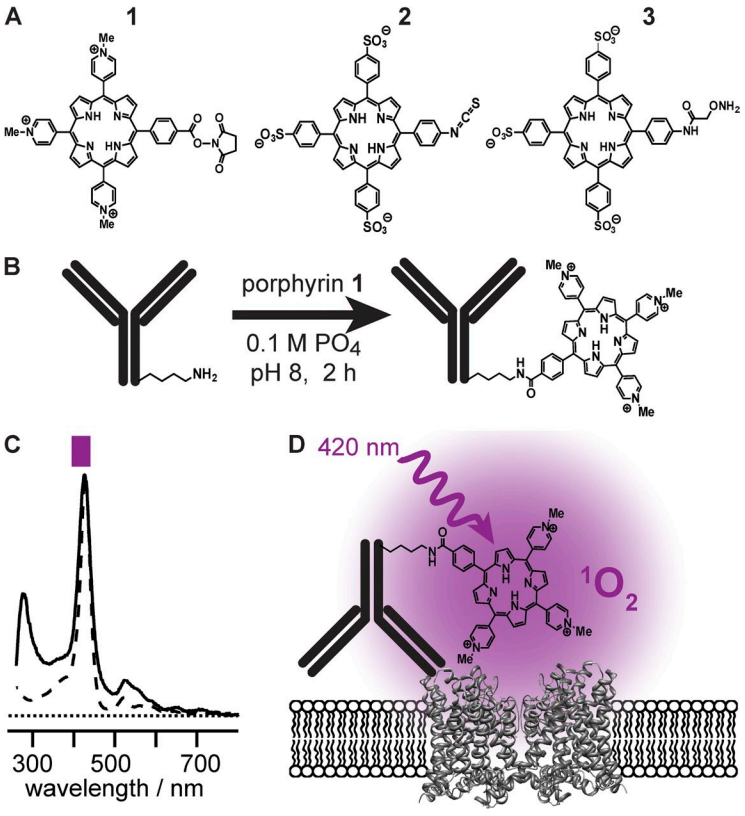

Figure 2. Porphyrin conjugation to mAbs. (A) Structures of porphyrins synthesized. (B) Schematic of porphyrin conjugation to a mAb. (C) Ultraviolet-visible absorption demonstrates that 420-nm absorbance is retained in conjugates. Spectrum of 1 (dashed line), scaled to match peak of αKv4.2•1 (solid line). Purple bar represents band-pass of illumination filter used in electrophysiology experiments. (D) Schematic of mAb-mediated photoablation.

Cell culture

CHO-K1 cells were maintained in Ham's F12 media (Gibco) containing 10% FBS (Hyclone) at 37°C in a 5% CO_2 atmosphere. A stable Kv4.2 CHO-K1 cell line was generated with Kv4.2ΔN2-31 (Shibata et al., 2003) subcloned into a tetracycline-inducible expression system (TREx CHO; Life Technologies). 2 d after transfection (Nucleofector; Lonza), 10 µg/ml blasticidin and 250 µg/ml zeocin were added to culture media. To induce channel expression for electrophysiological recording, 1 µg/ml tetracycline was added to the maintenance media for 10–20 h to induce a desirable amount of channel expression. The Kv2.1 TREx CHO cell line (Trapani and Korn, 2003) was cultured similarly and required 1 µg/ml tetracycline for 1–2 h for channel expression. Kv4.3/RGB4 (Rhodes et al., 2004) was transfected similarly with an EGFP/pMax vector (Lonza), and currents were recorded 40–70 h after transfection. Kv4.2 HEK cells expressed a Kv4.2-GFP construct (Shibata et al., 2003), stably transfected into HEK293 cells, and were maintained in DMEM media containing 10% FBS and 500 µg/ml G418 (Life Technologies). For electrical recording, cells were harvested by scraping in a PBS with 1 mM EDTA (Versene; Life Technologies), pelleted at 1,000 *g* for 2 min, resuspended in CHO-SFMII media (Life Technologies) supplemented with 25 mM HEPES, pH 7.3, and rolled in a polypropylene tube at room temperature until use.

Electrophysiology

Whole cell voltage-clamp recordings were used to measure currents from Kv channels. Aliquots of cell suspension were added to a recording chamber and rinsed with external solution 5 or more minutes before recording. The external (bath) solution contained (mM): 20 HEPES, 10 KOH, 117 NaCl, 2 $CaCl_2$, 2 $MgCl_2$, and 0.1 MgEDTA, adjusted to pH 7.3 with HCl. The internal (pipette) solution contained (mM): 50 KF, 70 KCl, 35 KOH, 5 EGTA, and 50 HEPES, adjusted to pH 7.3 with HCl. A calculated liquid junction potential of 9.6 mV was corrected. Pipette tip resistances with these solutions were <3 MΩ. Recordings were done at room temperature (22–24°C). Voltage clamp was achieved with an amplifier run by Patchmaster software (EPC-10; HEKA). The holding potential was −100 mV. Series resistance compensation was used when needed to constrain voltage error to <10 mV. When indicated, capacitance and ohmic leak were subtracted using a P/5 protocol. Recordings were low-pass filtered at 5 kHz and digitized at 100 kHz. All recordings were made after the addition of 0.1% BSA. Antibody–porphyrin conjugates were applied in external solution with 0.1% BSA at least 100 s before illumination, with light exposure kept to a minimum until illumination start. Antibodies were added by pipetting 100 µl of a 2× concentration into a recording chamber (R-24N; Warner) containing ∼100 µl of solution.

Illumination for photoablation was administered by manually shuttering the epifluorescence input into a microscope (Axiovert 100; Carl Zeiss). Light source was a 100-W mercury arc lamp filtered by a 395–440-nm excitation filter (Zeiss filter set at 05). Unless noted otherwise, a 10× objective (1020–863; Carl Zeiss) was used for illumination. The total illumination output of the objective was 8–12 mW, as measured by a photodiode (S130VC; Thorlabs) calibrated at 425 nm. lllumination was adjusted by eye to be homogeneous across the field of view, with the patch-clamped cell centered in the field of view and plane of focus on the greatest diameter of the cell membrane.

Data analysis

Analysis and graphing were performed with IgorPro software (WaveMetrics), which performs nonlinear least-squares fits using a Levenberg–Marquardt algorithm. K current photoablation was fit with an exponential decay function:

$$current = base + Ae^{-rate \cdot time}, \quad (1)$$

where *time* is the time elapsed since onset of illumination, *rate* is the photoablation rate, *A* is amplitude, and *base* is *current* remaining at *time* = ∞. The figure legends report *rate* ± SD and *f* ± SD, where *f* is the fraction of current ablated when *current* = *base*. When *rate* was so slow as to be poorly constrained (<0.01 s^{-1}), *base* was constrained to 0. This constraint did not alter the significance of any statistical comparisons. Significance was determined by rank using the nonparametric Mann–Whitney *U* test. Asterisks indicate $P < 0.05$. In the figures, electrophysiological current traces were digitally smoothed with a 2-kHz Gaussian filter. Error bars indicate mean ± SEM.

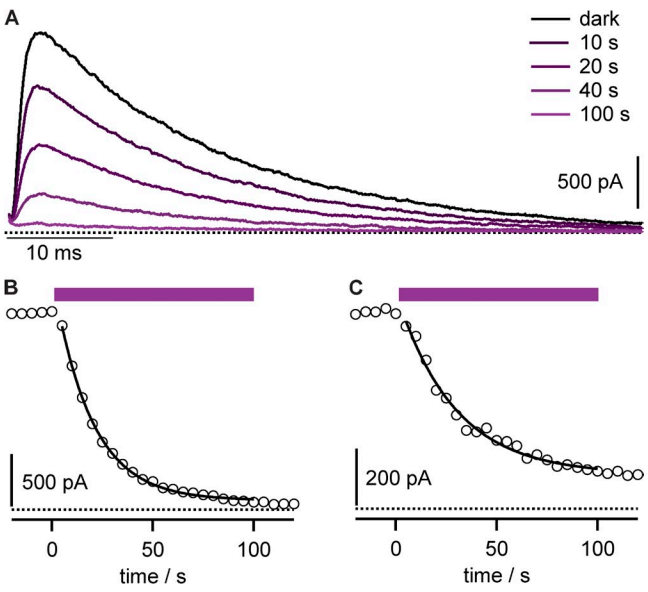

Figure 3. Anti-Kv4.2 mAb–porphyrin conjugate facilitates photoablation of K currents. (A) Kv4.2 currents during photoablation with 10 nM αKv4.2•1. Stimulatory pulses to 0 mV, with illumination beginning after time = 0. Data from CHO cell. (B) Circles, peak currents from cell in A. Purple bar indicates period of illumination. Line is fit of Eq. 1; *rate* = 0.053 ± 0.001 s^{-1} and *f* = 0.953 ± 0.004. (C) Peak Kv4.2 currents from cell similar to that in B, except conjugate was removed from bath solution for 2 min before illumination. Line is fit of Eq. 1; *rate* = 0.035 ± 0.003 s^{-1} and *f* = 0.82 ± 0.02.

RESULTS

Antibody–porphyrin conjugates facilitate targeted K current photoablation

Antibody–porphyrin conjugates were added to the external solution of patch-clamped cells heterologously expressing Kv channels. After a brief incubation period to allow antibodies to bind channel targets, photostimulation of the highest extinction coefficient absorption (Soret) band of the anti-Kv4.2 mAb–porphyrin 1 conjugate, αKv4.2•1 (Fig. 2 C), resulted in progressive inhibition of Kv4.2 current with photon dose (Fig. 3, A and B). This irreversible photoablation is consistent with oxidative damage to channels from diffusible reactive oxygen species generated by photostimulated porphyrin, such

as singlet oxygen, as schematized (Fig. 2 D). Photoablation was also apparent after washout of mAb conjugate (Fig. 3 C), consistent with the conjugate channel complex having a slow dissociation rate from the targeted channels.

The αKv4.2•1 porphyrin–mAb conjugates allowed selective photoablation of the targeted Kv channels. There was little photoablation of Kv4.3 or Kv2.1 in response to photon doses that eliminated Kv4.2 currents, suggesting that antibody targeting could direct the photoablation effect (Fig. 4). The effect of increasing photon dose was quantified as a photoablation rate, corresponding to the inverse time constant of current loss under our illumination conditions (Fig. 4 E). With prolonged illumination, current was gradually lost from the off-target Kv2.1 and Kv4.3 channels. This side effect indicated that although the anti-Kv antibody could direct photoablation to channels of interest, collateral damage also occurred. Alternate porphyrin chemistries were not as successful at enabling targeted photoablation. The mAb–porphyrin conjugates of the two anionic porphyrins synthesized (2 and 3) did not selectively ablate currents from the targeted Kv4.2 channel. Under more intense illumination, high photon doses yielded nonselective photoablation against all channels tested (Fig. 5). This suggests that the ability of the K57/1 antibody to recognize its epitope is compromised by attachment of the anionic conjugates. It is not clear why the anionic conjugates were not targeted as effectively as their cationic counterpart, αKv4.2•1. The weaker, nonselective effects of αKv4.2• and αKv4.2•3, together with the off-target effects of αKv4.2•1 on Kv2.1 and Kv4.3, demonstrate that a mechanism beyond antibody–epitope binding can also lead to photoablation. Yet, with this technique, nonselective side effects were dwarfed by selective antibody-guided photoablation of Kv currents.

To further test the mechanism of Kv subtype targeting, we probed the selectivity of mAb conjugates with a blocking peptide. Preincubation with soluble Kv4.2e peptide prevented binding of 5 nM anti-Kv4.2 mAb to its epitope, with an IC_{50} of 7 nM (Fig. 6, A and B). When mAb conjugates were preblocked with saturating concentrations of this soluble epitope, photoablation by the cationic porphyrin–antibody conjugate was reduced (Fig. 6 C). The αKv4.2•1 photoablation of Kv4.2 currents was not completely blocked by the antigenic peptide, with the residual photoablation refractory to increased concentrations of peptide blocker. The block of photoablation by peptide is consistent with our other findings, where a degree of off-target effects accompany antibody-guided photoablation.

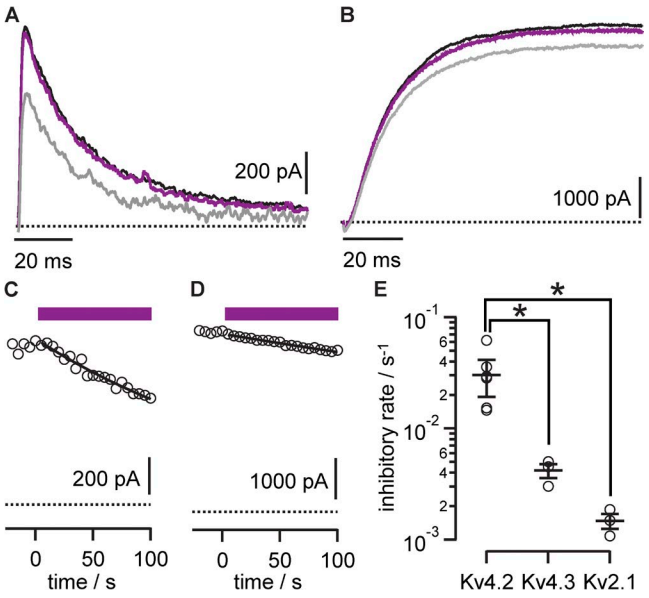

Figure 4. Anti-Kv4.2 porphyrin conjugates selectively photoinhibit Kv4.2. Photoablation of currents from Kv channels incubated with 10 nM αKv4.2•1. Data are from 0-mV pulses to patch-clamped whole CHO cells expressing the indicated channel. P/n leak subtraction was used to isolate K currents. (A) Limited inhibition of Kv4.3 currents. Black trace, before illumination; purple, after 10-s illumination; gray, after 100-s illumination. (B) Limited inhibition of Kv2.1 currents. Black trace, before illumination; purple, after 10-s illumination; gray, after 100-s illumination. (C) Circles, peak Kv4.3 currents. Purple bar indicates period of illumination. Line is fit of Eq. 1, with f = 1 and *rate* = 0.0045 ± 0.002 s^{-1}. (D) Circles, peak Kv2.1 currents; *rate* = 0.00108 ± 0.00004 s^{-1}. (E) Summary data of Kv subtype versus photoinhibitory rates derived from exponential fitting. Circles, individual cells. Kv4.2, $n = 6$; Kv4.3, $n = 3$; Kv2.1, $n = 3$.

Targeted photoablation reduces K current magnitude without altering gating

The details of mAb-guided photoablation were investigated to better understand how K current elimination

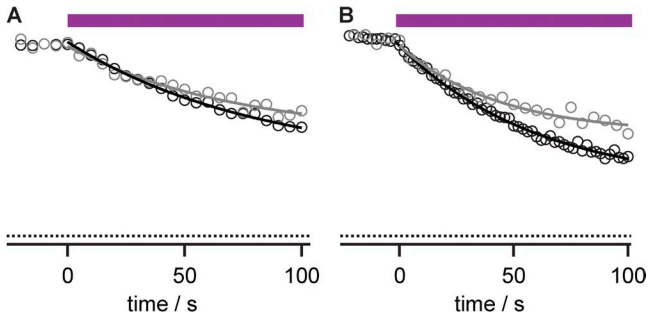

Figure 5. Anionic porphyrin conjugates do not facilitate selective photoablation. Data points are relative peak currents during 0-mV pulses to patch-clamped whole cells. Photon flux per unit area is approximately four times greater than in all other figures because of the 20× objective used. (A) Antibody–porphyrin 2 conjugate (20 nM) produced only nonselective photoablation of Kv currents. Black circles, Kv4.2 from HEK cells; *rate* = 0.012 ± 0.001 s^{-1} and f = 0.62 ± 0.04; gray circles, Kv2.1 from CHO cells; *rate* = 0.014 ± 0.004 s^{-1} and f = 0.48 ± 0.07. (B) Antibody–porphyrin 3 conjugate (20 nM) produced only nonselective photoablation of Kv currents. Black circles, Kv4.2; *rate* = 0.016 ± 0.001 s^{-1} and f = 0.75 ± 0.02; gray circles, Kv2.1; *rate* = 0.023 ± 0.004 s^{-1} and f = 0.49 ± 0.03.

occurs. The degree of photoablation was found to be dependent on the concentration of K57/1 antibody–porphyrin conjugate applied. Increased concentration resulted in photoablation of a greater fraction of K current (Fig. 7 A). During photostimulation, the rate of Kv4.2 current decay did not reveal a consistent difference between the conjugate concentrations tested (Fig. 7 B). The dynamics of remaining current elicited from cells after partial photoablation was similar to control. The sigmoid activation kinetics of Kv4.2 were similar to currents elicited before illumination, as were decaying tail currents from deactivation at negative voltages (Fig. 8 A), and inactivation (Fig. 3 A). The normal behavior of current remaining after photoablation contrasts with the progressive alteration of the channel gating machinery, as is seen with cyclic nucleotide–gated channels (Middendorf and Aldrich, 2000; Middendorf et al., 2000). The extent of Kv photoablation could be halted at a given level by the termination of illumination (Fig. 8 B), indicating that the physical processes leading to irreversible current loss are rapid events, rather than the triggering of a slow decay process.

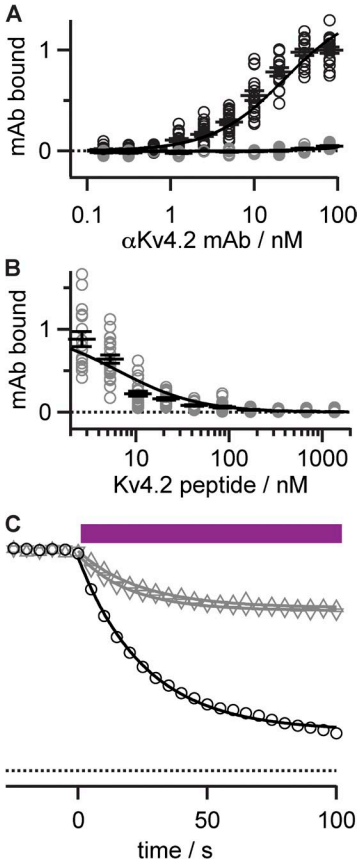

Figure 6. Block of photoablation by antigenic peptide. (A) Anti-Kv4.2 mAb binding to antigen is blocked by preincubation with soluble Kv4.2e peptide. ELISA binding assays. Abscissa is normalized to absorbance of 80 nM αKv4.2 mAb. Black circles, readings from individual wells; n = 16–21; gray circles, preincubation with 1 μM Kv4.2e blocking peptide; n = 5–15. Lines are fits of Langmuir binding isotherm: K_d αKv4.2 mAb = 23 ± 1 nM and +Kv4.2e peptide = 4,200 ± 2,600 nM. Bars, mean ± SEM. (B) Dose–response of antigenic peptide block. Gray circles, ELISA assays of 5 nM αKv4.2 mAb with increasing concentration of Kv4.2e peptide; n = 16–24. Fit of Langmuir isotherm has IC_{50} of 6.5 ± 1.1 nM. Bars, mean ± SEM. (C) Partial block of Kv4.2 photoablation by Kv4.2e peptide. Data points are relative peak currents from Kv4.2 CHO cells during 0-mV pulses. Purple bar indicates illumination. Circles, photoablation of Kv4.2 with 2.5 nM αKv4.2•1; *rate* = 0.039 ± 0.001 s^{-1} and f = 0.82 ± 0.01; triangles, same as circles except αKv4.2•1 was preincubated with 10 μM Kv4.2 peptide; *rate* = 0.041 ± 0.002 s^{-1} and f = 0.261 ± 0.003; triangles, 100 μM Kv4.2 peptide; *rate* = 0.050 ± 0.003 s^{-1} and f = 0.273 ± 0.004.

Photoablation inflicts collateral damage

The technique of porphyrin-mediated photoinhibition presents some technical difficulties that can complicate its application in the laboratory. Among these limitations are an endogenous photosensitivity of Kv channel currents and leak currents in cell membranes that are sometimes induced by photostimulation of porphyrin–mAb conjugates.

Limited Kv current photoablation was sometimes observed in the absence of porphyrins. Although photosensitivity of channels to the 420-nm illumination was usually not apparent without porphyrins added (Fig. 7 A), in certain cells there was a notable response to illumination, a particularly striking example of which is shown in Fig. 8 C. Although the endogenous photosensitivity complicates interpretation, it never approached the rate of photoablation observed with antibody–porphyrin conjugates (Fig. 7 B). It is not clear what endogenous chromophore may be mediating the response to illumination.

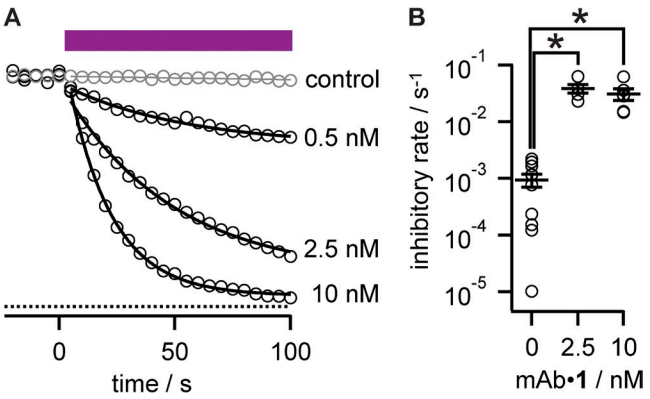

Figure 7. Dose dependence of photoablation. (A) Dose response of αKv4.2•1-mediated photoablation. Circles, relative peak currents from Kv4.2 CHO cells during 0-mV pulses with the indicated concentration of αKv4.2•1. Purple bar indicates illumination. Gray circles, 0 nM control; *rate* = 0.00015 ± 0.00004 s^{-1} and f = 1; black circles: 0.5 nM, *rate* = 0.019 ± 0.003 s^{-1} and f = 0.30 ± 0.02; 2.5 nM, *rate* = 0.021 ± 0.002 s^{-1} and f = 0.86 ± 0.02; 10 nM, *rate* = 0.052 ± 0.001 s^{-1} and f = 0.953 ± 0.004. (B) Summary data of αKv4.2•1 concentration versus photoinhibitory rates derived from exponential fitting. Circles, individual cells. 0 nM, n = 10; 2.5 nM, n = 5; 10 nM, n = 6.

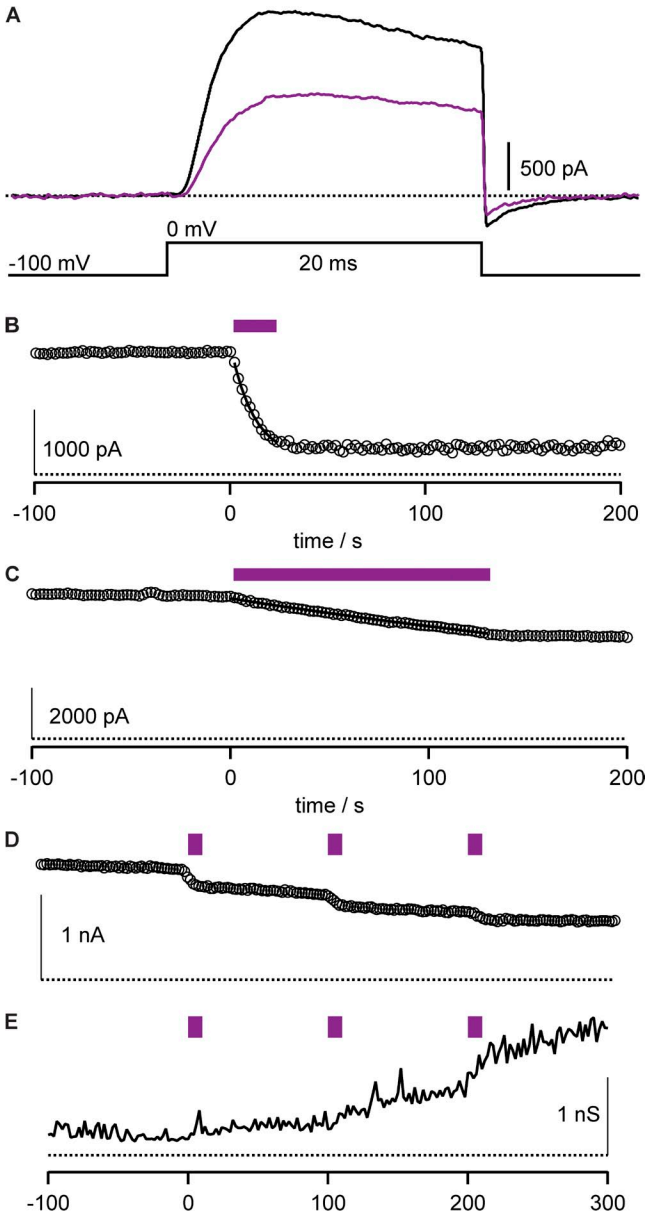

Figure 8. Properties of photoablation. Recordings from HEK cells expressing Kv4.2 with inactivation reduced. P/n subtraction was used to isolate K currents. (A) Detail of Kv4.2 current activation and deactivation. Black line, 10 nM αKv4.2•1 before illumination; purple line, after 10-s illumination. (B) The level of photoablation does not change after cessation of illumination. Circles, peak Kv4.2 currents during 0-mV pulses with 10 nM αKv4.2•1. Purple bar indicates illumination; *rate* = 0.083 ± 0.006 s^{-1} and f = 0.87 ± 0.03. (C) Example of endogenous photosensitivity. Circles, peak Kv4.2 currents during 0-mV pulses without any porphyrin–mAb conjugate. Purple bar indicates illumination; *rate* = 0.00221 ± 0.00002 s^{-1} and f = 1. (D) Sequential illumination pulses reveal that photoablation can be achieved through repetitive pulsing. Circles, peak Kv4.2 currents during 0-mV pulses with 10 nM αKv4.2•1. Purple bar indicates illumination. (E) Example of variable leak triggered by photoablation. Same cell as D. Input resistance measured by inward current at a holding potential of −100 mV.

In attempts to prevent background photoablation, a panel of reducing agents was added to the patch pipette, including 10 mM of reduced glutathione, 25 mM potassium ascorbate, 500 U/ml superoxide dismutase, 50 mM dithiothreitol, and 40 µM trolox C. These reducing agents were not effective at preventing background photoablation (unpublished data).

Another complicating facet of applying antibody–porphyrin-guided photoablation to patch-clamp studies was a variable level of photostimulated leak current that sometimes occurred. Leak currents occurred frequently, but inconsistently, after photostimulation of cells exposed to antibody–porphyrin conjugates. An example of the membrane leak sometimes accompanying photoablation is shown in Fig. 8 (D and E). Photostimulation inconsistently triggered an increased leakiness of the membrane that could further develop after cessation of illumination. A previous study using reactive oxygen–mediated photoablation of membrane proteins reported collateral damage to other cellular proteins (Guo et al., 2006), and the leak currents appearing in our experiments appear to be a manifestation of some form of collateral oxidative damage.

DISCUSSION

We have found that antibody-guided, porphyrin-mediated photoablation can select among Kv4 subtypes. This method of targeting channels yielded better specificity for Kv4.2 over Kv4.3 and Kv2.1 than any inhibitor we are aware of. Ablation of currents with conjugates of benign antibodies offers a new route toward pinpointing the molecular identity of endogenous channels underlying ionic current.

Porphyrin-conjugated derivatives of an anti-Kv mAb imbued photoablation specificity against a targeted Kv channel. This method also inflicted collateral damage against other channels and likely the cell membrane itself. The mechanism of collateral damage is unclear. We speculate that it is caused by an innate affinity of porphyrins for cell membranes, resulting in nonspecific adsorption of porphyrin–mAb conjugates to cell surfaces. Upon photostimulation, singlet oxygen from the adsorbed conjugates could harm other channels, damage the membrane to increase electrical leak, and inflict additional undetected forms of oxidative damage to the cell. This collateral damage is consistent with side effects noted by Guo et al. (2006) when photostimulating fluorescein conjugates on cell surfaces. Nonetheless, porphyrin conjugates have been useful in demonstrating the concept of antibody-guided Kv inhibition. This strategy could be improved upon by conjugating less technically problematic inhibitors.

We are currently working to conjugate promiscuous inhibitors of Kv channels to anti-Kv mAbs while retaining the function of both components. The ability of

benign antibodies to deliver inhibitory payloads to Kv channels is clear. Antibody-guided channel modulators could provide the experimental tools needed to reveal the specific physiological roles each Kv subunit is fulfilling in the body.

We are grateful to Dr. Leah Witus for inspiring this project. We thank Jordy Hsiao, Olga Lenkov, and Kenneth Eum for technical assistance, as well as Dr. Milena Menegola for brain immunohistochemistry.

This research was supported by National Institutes of Health National Institute of Neurological Disorders and Stroke grant R01NS042225, supplement R01NS042225-09S1 (to J.S. Trimmer), and American Heart Association grant 10SDG4220047 (to J.T. Sack).

Author Contributions: J.T. Sack, N. Stephanopoulos, and J.S. Trimmer generated reagents; J.T. Sack, D.C. Austin, and J.S. Trimmer performed experiments; J.T. Sack and D.C. Austin analyzed data; J.T. Sack, J.S. Trimmer, N. Stephanopoulos, and M.B. Francis wrote the manuscript.

Kenton J Swartz served as editor.

Submitted: 8 May 2013
Accepted: 19 July 2013

REFERENCES

Agostinis, P., K. Berg, K.A. Cengel, T.H. Foster, A.W. Girotti, S.O. Gollnick, S.M. Hahn, M.R. Hamblin, A. Juzeniene, D. Kessel, et al. 2011. Photodynamic therapy of cancer: an update. *CA Cancer J. Clin.* 61:250–281. http://dx.doi.org/10.3322/caac.20114

Alonso, C.M., A. Palumbo, A.J. Bullous, F. Pretto, D. Neri, and R.W. Boyle. 2010. Site-specific and stoichiometric conjugation of cationic porphyrins to antiangiogenic monoclonal antibodies. *Bioconjug. Chem.* 21:302–313. http://dx.doi.org/10.1021/bc9003537

Amarillo, Y., J.A. De Santiago-Castillo, K. Dougherty, J. Maffie, E. Kwon, M. Covarrubias, and B. Rudy. 2008. Ternary Kv4.2 channels recapitulate voltage-dependent inactivation kinetics of A-type K^+ channels in cerebellar granule neurons. *J. Physiol.* 586:2093–2106. http://dx.doi.org/10.1113/jphysiol.2007.150540

Antonucci, D.E., S.T. Lim, S. Vassanelli, and J.S. Trimmer. 2001. Dynamic localization and clustering of dendritic Kv2.1 voltage-dependent potassium channels in developing hippocampal neurons. *Neuroscience.* 108:69–81. http://dx.doi.org/10.1016/S0306-4522(01)00476-6

Baumgart, F., A. Rossi, and A.S. Verkman. 2012. Light inactivation of water transport and protein–protein interactions of aquaporin–Killer Red chimeras. *J. Gen. Physiol.* 139:83–91. http://dx.doi.org/10.1085/jgp.201110712

Beck, S., T. Sakurai, B.K. Eustace, G. Beste, R. Schier, F. Rudert, and D.G. Jay. 2002. Fluorophore-assisted light inactivation: a high-throughput tool for direct target validation of proteins. *Proteomics.* 2:247–255. http://dx.doi.org/10.1002/1615-9861(200203)2:3<247::AID-PROT247>3.0.CO;2-K

Beeton, C., H. Wulff, N.E. Standifer, P. Azam, K.M. Mullen, M.W. Pennington, A. Kolski-Andreaco, E. Wei, A. Grino, D.R. Counts, et al. 2006. Kv1.3 channels are a therapeutic target for T cell-mediated autoimmune diseases. *Proc. Natl. Acad. Sci. USA.* 103:17414–17419. http://dx.doi.org/10.1073/pnas.0605136103

Bonnett, R. 1995. Photosensitizers of the porphyrin and phthalocyanine series for photodynamic therapy. *Chem. Soc. Rev.* 24:19–33. http://dx.doi.org/10.1039/cs9952400019

Burkhalter, A., Y. Gonchar, R.L. Mellor, and J.M. Nerbonne. 2006. Differential expression of I(A) channel subunits Kv4.2 and Kv4.3 in mouse visual cortical neurons and synapses. *J. Neurosci.* 26:12274–12282. http://dx.doi.org/10.1523/JNEUROSCI.2599-06.2006

Dallas, M.L., S.A. Deuchars, and J. Deuchars. 2010. Immunopharmacology: utilizing antibodies as ion channel modulators. *Expert Rev Clin Pharmacol.* 3:281–289. http://dx.doi.org/10.1586/ecp.10.18

DeCoursey, T.E., K.G. Chandy, S. Gupta, and M.D. Cahalan. 1984. Voltage-gated K^+ channels in human T lymphocytes: a role in mitogenesis? *Nature.* 307:465–468. http://dx.doi.org/10.1038/307465a0

Endo, M., M. Fujitsuka, and T. Majima. 2007. Porphyrin light-harvesting arrays constructed in the recombinant tobacco mosaic virus scaffold. *Chemistry.* 13:8660–8666. http://dx.doi.org/10.1002/chem.200700895

Gardoni, F., D. Mauceri, E. Marcello, C. Sala, M. Di Luca, and A. Jeromin. 2007. SAP97 directs the localization of Kv4.2 to spines in hippocampal neurons: regulation by CaMKII. *J. Biol. Chem.* 282:28691–28699. http://dx.doi.org/10.1074/jbc.M701899200

Gilmore, J.M., R.A. Scheck, A.P. Esser-Kahn, N.S. Joshi, and M.B. Francis. 2006. N-terminal protein modification through a biomimetic transamination reaction. *Angew. Chem. Int. Ed. Engl.* 45:5307–5311. http://dx.doi.org/10.1002/anie.200600368

Gómez-Varela, D., E. Zwick-Wallasch, H. Knötgen, A. Sánchez, T. Hettmann, D. Ossipov, R. Weseloh, C. Contreras-Jurado, M. Rothe, W. Stühmer, and L.A. Pardo. 2007. Monoclonal antibody blockade of the human Eag1 potassium channel function exerts antitumor activity. *Cancer Res.* 67:7343–7349. http://dx.doi.org/10.1158/0008-5472.CAN-07-0107

Grissmer, S., B. Dethlefs, J.J. Wasmuth, A.L. Goldin, G.A. Gutman, M.D. Cahalan, and K.G. Chandy. 1990. Expression and chromosomal localization of a lymphocyte K^+ channel gene. *Proc. Natl. Acad. Sci. USA.* 87:9411–9415. http://dx.doi.org/10.1073/pnas.87.23.9411

Guo, W., W.E. Jung, C. Marionneau, F. Aimond, H. Xu, K.A. Yamada, T.L. Schwarz, S. Demolombe, and J.M. Nerbonne. 2005. Targeted deletion of Kv4.2 eliminates I(to,f) and results in electrical and molecular remodeling, with no evidence of ventricular hypertrophy or myocardial dysfunction. *Circ. Res.* 97:1342–1350. http://dx.doi.org/10.1161/01.RES.0000196559.63223.aa

Guo, J., H. Chen, H.L. Puhl III, and S.R. Ikeda. 2006. Fluorophore-assisted light inactivation produces both targeted and collateral effects on N-type calcium channel modulation in rat sympathetic neurons. *J. Physiol.* 576:477–492. http://dx.doi.org/10.1113/jphysiol.2006.113068

Gutman, G.A., K.G. Chandy, S. Grissmer, M. Lazdunski, D. McKinnon, L.A. Pardo, G.A. Robertson, B. Rudy, M.C. Sanguinetti, W. Stühmer, and X. Wang. 2005. International Union of Pharmacology. LIII. Nomenclature and molecular relationships of voltage-gated potassium channels. *Pharmacol. Rev.* 57:473–508. http://dx.doi.org/10.1124/pr.57.4.10

Hammond, R.S., L. Lin, M.S. Sidorov, A.M. Wikenheiser, and D.A. Hoffman. 2008. Protein kinase A mediates activity-dependent Kv4.2 channel trafficking. *J. Neurosci.* 28:7513–7519. http://dx.doi.org/10.1523/JNEUROSCI.1951-08.2008

Jiang, Y., A. Lee, J. Chen, V. Ruta, M. Cadene, B.T. Chait, and R. MacKinnon. 2003. X-ray structure of a voltage-dependent K^+ channel. *Nature.* 423:33–41. http://dx.doi.org/10.1038/nature01580

Kaczorowski, G.J., O.B. McManus, B.T. Priest, and M.L. Garcia. 2008. Ion channels as drug targets: The next GPCRs. *J. Gen. Physiol.* 131:399–405. http://dx.doi.org/10.1085/jgp.200709946

Kim, J., S.C. Jung, A.M. Clemens, R.S. Petralia, and D.A. Hoffman. 2007. Regulation of dendritic excitability by activity-dependent trafficking of the A-type K^+ channel subunit Kv4.2 in hippocampal neurons. *Neuron.* 54:933–947. http://dx.doi.org/10.1016/j.neuron.2007.05.026

Lee, J., P. Yu, X. Xiao, and T. Kodadek. 2008. A general system for evaluating the efficiency of chromophore-assisted light inactivation (CALI) of proteins reveals Ru(II) tris-bipyridyl as an unusually efficient "warhead". *Mol. Biosyst.* 4:59–65. http://dx.doi.org/10.1039/b712307h

Lim, S.T., D.E. Antonucci, R.H. Scannevin, and J.S. Trimmer. 2000. A novel targeting signal for proximal clustering of the Kv2.1 K^+ channel in hippocampal neurons. *Neuron.* 25:385–397. http://dx.doi.org/10.1016/S0896-6273(00)80902-2

Lin, C.S., R.C. Boltz, J.T. Blake, M. Nguyen, A. Talento, P.A. Fischer, M.S. Springer, N.H. Sigal, R.S. Slaughter, M.L. Garcia, et al. 1993. Voltage-gated potassium channels regulate calcium-dependent pathways involved in human T lymphocyte activation. *J. Exp. Med.* 177:637–645. http://dx.doi.org/10.1084/jem.177.3.637

Menegola, M., and J.S. Trimmer. 2006. Unanticipated region- and cell-specific downregulation of individual KChIP auxiliary subunit isotypes in Kv4.2 knock-out mouse brain. *J. Neurosci.* 26:12137–12142. http://dx.doi.org/10.1523/JNEUROSCI.2783-06.2006

Middendorf, T.R., and R.W. Aldrich. 2000. Effects of ultraviolet modification on the gating energetics of cyclic nucleotide–gated channels. *J. Gen. Physiol.* 116:253–282. http://dx.doi.org/10.1085/jgp.116.2.253

Middendorf, T.R., R.W. Aldrich, and D.A. Baylor. 2000. Modification of cyclic nucleotide–gated ion channels by ultraviolet light. *J. Gen. Physiol.* 116:227–252. http://dx.doi.org/10.1085/jgp.116.2.227

Murakoshi, H., and J.S. Trimmer. 1999. Identification of the Kv2.1 K^+ channel as a major component of the delayed rectifier K^+ current in rat hippocampal neurons. *J. Neurosci.* 19:1728–1735.

Palumbo, A., F. Hauler, P. Dziunycz, K. Schwager, A. Soltermann, F. Pretto, C. Alonso, G.F. Hofbauer, R.W. Boyle, and D. Neri. 2011. A chemically modified antibody mediates complete eradication of tumours by selective disruption of tumour blood vessels. *Br. J. Cancer.* 104:1106–1115. http://dx.doi.org/10.1038/bjc.2011.78

Redmond, R.W., and J.N. Gamlin. 1999. A compilation of singlet oxygen yields from biologically relevant molecules. *Photochem. Photobiol.* 70:391–475.

Rhodes, K.J., and J.S. Trimmer. 2008. Antibody-based validation of CNS ion channel drug targets. *J. Gen. Physiol.* 131:407–413. http://dx.doi.org/10.1085/jgp.200709926

Rhodes, K.J., K.I. Carroll, M.A. Sung, L.C. Doliveira, M.M. Monaghan, S.L. Burke, B.W. Strassle, L. Buchwalder, M. Menegola, J. Cao, et al. 2004. KChIPs and Kv4 alpha subunits as integral components of A-type potassium channels in mammalian brain. *J. Neurosci.* 24:7903–7915. http://dx.doi.org/10.1523/JNEUROSCI.0776-04.2004

Scheck, R.A., and M.B. Francis. 2007. Regioselective labeling of antibodies through N-terminal transamination. *ACS Chem. Biol.* 2:247–251. http://dx.doi.org/10.1021/cb6003959

Shi, G., A.K. Kleinklaus, N.V. Marrion, and J.S. Trimmer. 1994. Properties of Kv2.1 K^+ channels expressed in transfected mammalian cells. *J. Biol. Chem.* 269:23204–23211.

Shibata, R., H. Misonou, C.R. Campomanes, A.E. Anderson, L.A. Schrader, L.C. Doliveira, K.I. Carroll, J.D. Sweatt, K.J. Rhodes, and J.S. Trimmer. 2003. A fundamental role for KChIPs in determining the molecular properties and trafficking of Kv4.2 potassium channels. *J. Biol. Chem.* 278:36445–36454. http://dx.doi.org/10.1074/jbc.M306142200

Sjoback, R., J. Nygren, and M. Kubista. 1998. Characterization of fluorescein-oligonucleotide conjugates and measurement of local electrostatic potential. *Biopolymers.* 46:445–453.

Smith, K., N. Malatesti, N. Cauchon, D. Hunting, R. Lecomte, J.E. van Lier, J. Greenman, and R.W. Boyle. 2011. Mono- and tri-cationic porphyrin-monoclonal antibody conjugates: photodynamic activity and mechanism of action. *Immunology.* 132:256–265. http://dx.doi.org/10.1111/j.1365-2567.2010.03359.x

Stephanopoulos, N., Z.M. Carrico, and M.B. Francis. 2009. Nanoscale integration of sensitizing chromophores and porphyrins with bacteriophage MS2. *Angew. Chem. Int. Ed. Engl.* 48:9498–9502. http://dx.doi.org/10.1002/anie.200902727

Stephanopoulos, N., G.J. Tong, S.C. Hsiao, and M.B. Francis. 2010. Dual-surface modified virus capsids for targeted delivery of photodynamic agents to cancer cells. *ACS Nano.* 4:6014–6020. http://dx.doi.org/10.1021/nn1014769

Tarcha, E.J., V. Chi, E.J. Muñoz-Elías, D. Bailey, L.M. Londono, S.K. Upadhyay, K. Norton, A. Banks, I. Tjong, H. Nguyen, et al. 2012. Durable pharmacological responses from the peptide ShK-186, a specific Kv1.3 channel inhibitor that suppresses T cell mediators of autoimmune disease. *J. Pharmacol. Exp. Ther.* 342:642–653. http://dx.doi.org/10.1124/jpet.112.191890

Tiffany, A.M., L.N. Manganas, E. Kim, Y.P. Hsueh, M. Sheng, and J.S. Trimmer. 2000. PSD-95 and SAP97 exhibit distinct mechanisms for regulating K^+ channel surface expression and clustering. *J. Cell Biol.* 148:147–158. http://dx.doi.org/10.1083/jcb.148.1.147

Tomé, J.P., M.G. Neves, A.C. Tomé, J.A. Cavaleiro, M. Soncin, M. Magaraggia, S. Ferro, and G. Jori. 2004. Synthesis and antibacterial activity of new poly-S-lysine-porphyrin conjugates. *J. Med. Chem.* 47:6649–6652. http://dx.doi.org/10.1021/jm040802v

Tour, O., R.M. Meijer, D.A. Zacharias, S.R. Adams, and R.Y. Tsien. 2003. Genetically targeted chromophore-assisted light inactivation. *Nat. Biotechnol.* 21:1505–1508. http://dx.doi.org/10.1038/nbt914

Trapani, J.G., and S.J. Korn. 2003. Control of ion channel expression for patch clamp recordings using an inducible expression system in mammalian cell lines. *BMC Neurosci.* 4:15. http://dx.doi.org/10.1186/1471-2202-4-15

Trimmer, J.S. 1991. Immunological identification and characterization of a delayed rectifier K^+ channel polypeptide in rat brain. *Proc. Natl. Acad. Sci. USA.* 88:10764–10768. http://dx.doi.org/10.1073/pnas.88.23.10764

Trimmer, J.S., I.S. Trowbridge, and V.D. Vacquier. 1985. Monoclonal antibody to a membrane glycoprotein inhibits the acrosome reaction and associated Ca^{2+} and H^+ fluxes of sea urchin sperm. *Cell.* 40:697–703. http://dx.doi.org/10.1016/0092-8674(85)90218-1

Vacher, H., D.P. Mohapatra, and J.S. Trimmer. 2008. Localization and targeting of voltage-dependent ion channels in mammalian central neurons. *Physiol. Rev.* 88:1407–1447. http://dx.doi.org/10.1152/physrev.00002.2008

Vegh, R.B., K.M. Solntsev, M.K. Kuimova, S. Cho, Y. Liang, B.L. Loo, L.M. Tolbert, and A.S. Bommarius. 2011. Reactive oxygen species in photochemistry of the red fluorescent protein "Killer Red". *Chem. Commun. (Camb.).* 47:4887–4889. http://dx.doi.org/10.1039/c0cc05713d

Verlhac, J., A. Gaudemer, and I. Kraljic. 1984. Water-soluble porphyrins and metalloporphyrins as photosensitizers in aerated aqueous solutions. I: Detection and determination of quantum yield of formation of singlet oxygen. *Nouveau Journal de Chimie.* 8:401–406.

Wilkinson, F., W.P. Helman, and A.B. Ross. 1993. Quantum yields for the photosensitized formation of the lowest electronically excited singlet state of molecular oxygen in solution. *J. Phys. Chem. Ref. Data.* 22:113–263.

Xu, S.Z., G. Boulay, R. Flemming, and D.J. Beech. 2006. E3-targeted anti-TRPC5 antibody inhibits store-operated calcium entry in freshly isolated pial arterioles. *Am. J. Physiol. Heart Circ. Physiol.* 291:H2653–H2659. http://dx.doi.org/10.1152/ajpheart.00495.2006

Yang, X.F., Y. Yang, Y.T. Lian, Z.H. Wang, X.W. Li, L.X. Cheng, J.P. Liu, Y.F. Wang, X. Gao, Y.H. Liao, et al. 2012. The antibody targeting the E314 peptide of human Kv1.3 pore region serves as a novel, potent and specific channel blocker. *PLoS ONE.* 7:e36379. http://dx.doi.org/10.1371/journal.pone.0036379

Zhou, B.Y., W. Ma, and X.Y. Huang. 1998. Specific antibodies to the external vestibule of voltage-gated potassium channels block current. *J. Gen. Physiol.* 111:555–563. http://dx.doi.org/10.1085/jgp.111.4.555